Canopy Height Estimation in Mediterranean Forests of Spain With TanDEM-X Data

Cristina Gómez, Juan M. Lopez-Sanchez, *Senior Member, IEEE*, Noelia Romero-Puig, *Student Member, IEEE*, Jianjun Zhu, Haiqiang Fu, Wenjie He, Yanzhou Xie, and Qinghua Xie

***Abstract*—Canopy height is an essential feature in forest inventory, and for the assessment of biomass and carbon budgets. Spatially explicit maps of forest height over large areas can be derived from satellite synthetic aperture radar data. We aimed to evaluate the capacity of TanDEM-X (TDX) data to assess canopy height in Mediterranean forests of Spain, which are of relatively short height (typically < 20 m), diverse in species and structure, and adapted to summer drought. Interferogram coherence was retrieved from single-pol image pairs. Forest height estimation was carried out by previously fitting a sinc-type function, with two empirical parameters, to the data measured. Six types of forest were defined to assess the convenience of stratification for model implementation. The influence of terrain slope, forest type, and interferometric baseline on model performance was evaluated, and a strategy for large area mapping was proposed and tested. TDX-derived heights were compared to a contemporaneous LiDAR-derived canopy height model for assessment of quality. Results limited to slopes below 10° provided the best results, reaching $R^2 = 0.91$ and root-mean-square error $= 1.24$ m in one of the study sites. However, in some areas the results were much worse, especially in regions characterized by rugged terrain with broadleaved species. This work demonstrates the feasibility of deriving a forest height map over the entire area of Spain from TDX data. Stratification per slope interval and selection of long interferometric baselines are recommended.**

***Index Terms*—Forest canopy height, Mediterranean forest, Spain, synthetic aperture radar (SAR) interferometry, TanDEM-X (TDX).**

Manuscript received October 10, 2020; revised January 12, 2021; accepted February 15, 2021. Date of publication February 19, 2021; date of current version March 17, 2021. This work was supported in part by the Spanish Ministry of Science, Innovation, and University and EU EFDR funds under Project TEC2017-85244-C2-1-P, and in part by the National Natural Science Foundation of China under Grant 41820104005, Grant 41804004, and Grant 41904004. The work of Cristina Gómez was supported under Project FORESTCHANGE (AGL2016-76769-C2-1-R) funded by the Spanish Ministry of Science, Innovation, and University. *(Corresponding author: Juan M. Lopez-Sanchez.)*

Cristina Gómez was with the INIA-CIFOR, 28040 Madrid, Spain. She is now with the iuFOR-EiFAB Campus de Soria, University of Valladolid, 42004 Soria, Spain, and also with the University of Aberdeen, Aberdeen, AB24 3UE, Scotland, U.K. (e-mail: cristina.gomez@cesefor.com).

Juan M. Lopez-Sanchez and Noelia Romero-Puig are with the Signals, Systems and Telecommunications Group, Instituto Universitario de Investigación Informática, University of Alicante, 03080 Alicante, Spain (e-mail: juanma.lopez@ua.es; noelia.romero@ua.es).

Jianjun Zhu, Haiqiang Fu, Wenjie He, and Yanzhou Xie are with the School of Geoscience and Info-Physics, Central South University, Changsha 410083, China (e-mail: zjj@csu.edu.cn; haiqiangfu@csu.edu.cn; hewenjie@csu.edu.cn; david_tse@csu.edu.cn).

Qinghua Xie is with the School of Geography and Information Engineering, China University of Geosciences, Wuhan 430074, China (e-mail: xieqh@cug.edu.cn).

Digital Object Identifier 10.1109/JSTARS.2021.3060691

I. Introduction

FOREST canopy height is a key parameter in forest inventory [1], for estimation of biomass and carbon storage [2], for assessment of essential biodiversity variables [3], and to enable periodical reports and informed management decisions [4]. Estimating forest height over large areas requires modeling [5], [6] and benefits from complete coverage of spatially explicit data, only possible with satellite acquisitions [7]–[9].

Active sensors are better suited than passive counterparts for estimation of forest height [10], [11]. Aerial laser scanner, i.e., LiDAR systems provide forest height estimations with unsurpassed accuracy. Unfortunately, the resulting maps are not refreshed frequently due to the high economical costs of the associated flight campaigns. Satellite-based forest canopy height has been estimated globally from the Geoscience Laser Altimeter System LiDAR aboard the Ice, Cloud and land Elevation Satellite (ICESat) and the Advanced Topographic Laser Altimeter System instrument on ICESat-2 with sampling strategies [7], [8], [12], [13]. Since 2019, the Global Ecosystem Dynamics Investigation (GEDI) onboard the International Space Station, collects LiDAR data between 51.6°N and 51.6°S with an optimized configuration for retrieval of vegetation vertical structure [14]. GEDI mission has a sampling strategy that requires support from other spatially comprehensive datasets to extrapolate height estimations globally [15]. Global maps of forest height support global climate and sustainable development initiatives but have limited accuracy and resolution for national resource inventory.

An alternative to LiDAR data for estimation of canopy height is provided by spaceborne synthetic aperture radar (SAR) systems, which have continuous and cost-effective global coverage at high temporal and spatial resolution [16], [17]. The TanDEM-X dual satellite mission (hereafter TDX) was launched by the German Aerospace Center (DLR) in 2010, operates at *X*-band (3.1 cm wavelength) and acquires single polarized data in its standard mode (with horizontally polarized waves, i.e., HH). TDX enables SAR interferometry with null temporal decorrelation thanks to the orbital configuration of the twin satellites [18] and it is, therefore, a good alternative for estimation of forest canopy height. TDX has been used for the estimation of forest height in temperate [19], tropical [20], and boreal forests [21] exploiting the relationship between interferometric coherence and canopy height [22].

In order to retrieve forest height from the interferometric coherence measured by TDX, a simple physical model is inverted.

The most typical model in this application is the random volume over ground (RVoG) [23], [24], which provides an expression of the complex interferometric coherence as a function of a few parameters, namely: underlying topography, vegetation height, wave extinction in the vegetation volume, and ground-to-volume backscatter ratio. The interferometric phase could be used for height inversion provided that the topographic phase was known, but a good quality DTM would be required. Instead, the coherence amplitude does not depend on the knowledge of the topographic phase and, therefore, has been widely used for estimating forest height [19], [25], [26]. Unfortunately, the RVoG model must be simplified to enable the forest height inversion, for which the extinction and the ground-to-volume ratio are assumed to be known. The assumptions depend on the forest type and the acquisition configuration, mainly incidence angle, baseline, and local slope, so their generalization is a challenging task [19], [27].

Mediterranean forests extend over 88 million ha in 27 countries, according to FAO statistics [28]. More than 20% of the Mediterranean forest land lays in Spain [29], where forest land is in expansion since 1990 as a result of the European Common Agriculture Policy and forest regeneration in rural areas following abandonment [30], [31]. Mediterranean forests are characterized by the presence of tree species adapted to summer drought [32], with relatively short heights and less dense if compared with forests in other biomes. Furthermore, Spanish forests distribute on mountain areas with very strong topographic relief.

The goal of the project, whose initial results are illustrated here, is to assess, for the first time, the capacity of interferometric techniques employing TDX data for estimation of forest canopy height in Mediterranean environments. Our specific objectives in this work are as follows:

1) to test the capacity of TDX data for estimation of forest height in the Spanish forests;
2) to identify the factors affecting the accuracy in estimation of forest height, and the need of stratification for the development of a large area map; and
3) to demonstrate the feasibility of mapping large areas of forest height in Spain.

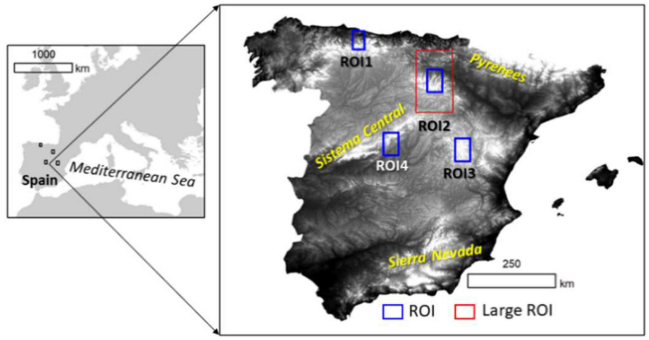

Fig. 1. Location of the study area in the Mediterranean basin, and digital elevation map of Spain (without the Canary Islands), in which the location of the four regions of interest (ROIs) is depicted.

TABLE I
FOREST TYPES DEFINED FOR STRATIFICATION PURPOSES

Name	Forest type	Dominant species	Characteristics
Conifer 1	Pines	*P. sylvestris, P. pinaster, P. nigra, P. pinea, P. halepensis, P. uncinata*	• Evergreen needled species • Dense stands • Maximum tree height ~ 35 m
Conifer 2	Pines & other coniferous	*Pinus spp., Juniperus spp.,*	• Evergreen needled / non-needled species • Variable density of stands • Typical maximum stand height ~ 15 m
Broad 1	Temperate broadleaved	*Quercus robur, Q. petraea, Fagus sylvatica, Betula spp., Fraxinus spp.*	• Mainly winter-deciduous species • Relatively dense stands • Maximum tree height ~ 33 m
Broad 2	Mediterranean broadleaved	*Quercus ilex, Q. pyrenaica, Q. faginea, Q. suber*	• Mainly evergreen species • Variable density of stands • Maximum tree height ~ 28 m
Mixed 1	Coniferous & broadleaved temperate	*Pinus spp., Quercus spp., Fagus sylvatica*	• Conifers and broadleaved species intermingled • Typical maximum stand height ~ 18 m
Mixed 2	Coniferous & broadleaved Mediterranean	*Pinus spp., Quercus spp.*	• Conifers and broadleaved species intermingled • Typical maximum stand height ~ 15 m

Reference data from the Spanish MFE50 and NFI3.

II. MATERIALS AND METHODS

A. Study Area

The Spanish land has strong topographic variations, with the main mountain ranges oriented in E–W direction and peaks reaching altitudes of 3479 m in the Sierra Nevada and 3404 m in the Pyrenees (see Fig. 1). Forests in Spain have an overall complex structure and are variable in composition, comprising more than 150 tree species [33]. *Pinus*, *Quercus*, *Fagus*, *Abies,* or *Betula* species are dominant in mountain areas. Natural forests structurally complex coexist with very homogeneous coniferous reforestations from the mid-20th century in the southern region and with fast-growing plantations of *Pinus* and Eucalyptus in the Northern region. Open woodlands named *dehesas*, and dense forests dominated by *Quercus* and *Fraxinus* spread over the plains, along with pinewoods managed for production of timber, fruit, and resin, and productive plantations of *Populus* and Eucalyptus [34]. Overall, tree heights are shorter than in other biomes, with >90% of trees measured by the third rotation of the National Forest Inventory (NFI3) below 20 m. To facilitate stratification into forest types of similar ecological and structural characteristics, reference data from the Spanish Forest Map (MFE50 [35]) were reclassified and all forests were grouped into six classes, which were defined attending to the dominance of tree species, tree density, and ecological conditions (see Table I). We expect these six classes of forest, or at least some of them, to respond differently in the TDX imagery, and hence in the canopy height modeling and inversion.

Four test sites or ROIs of 2500 km^2 on average were selected with the objective of representing most of the forest features found in Spain and, also importantly, with diverse proportion and distribution of forest types [see Fig. 2(a)]. Forest stands

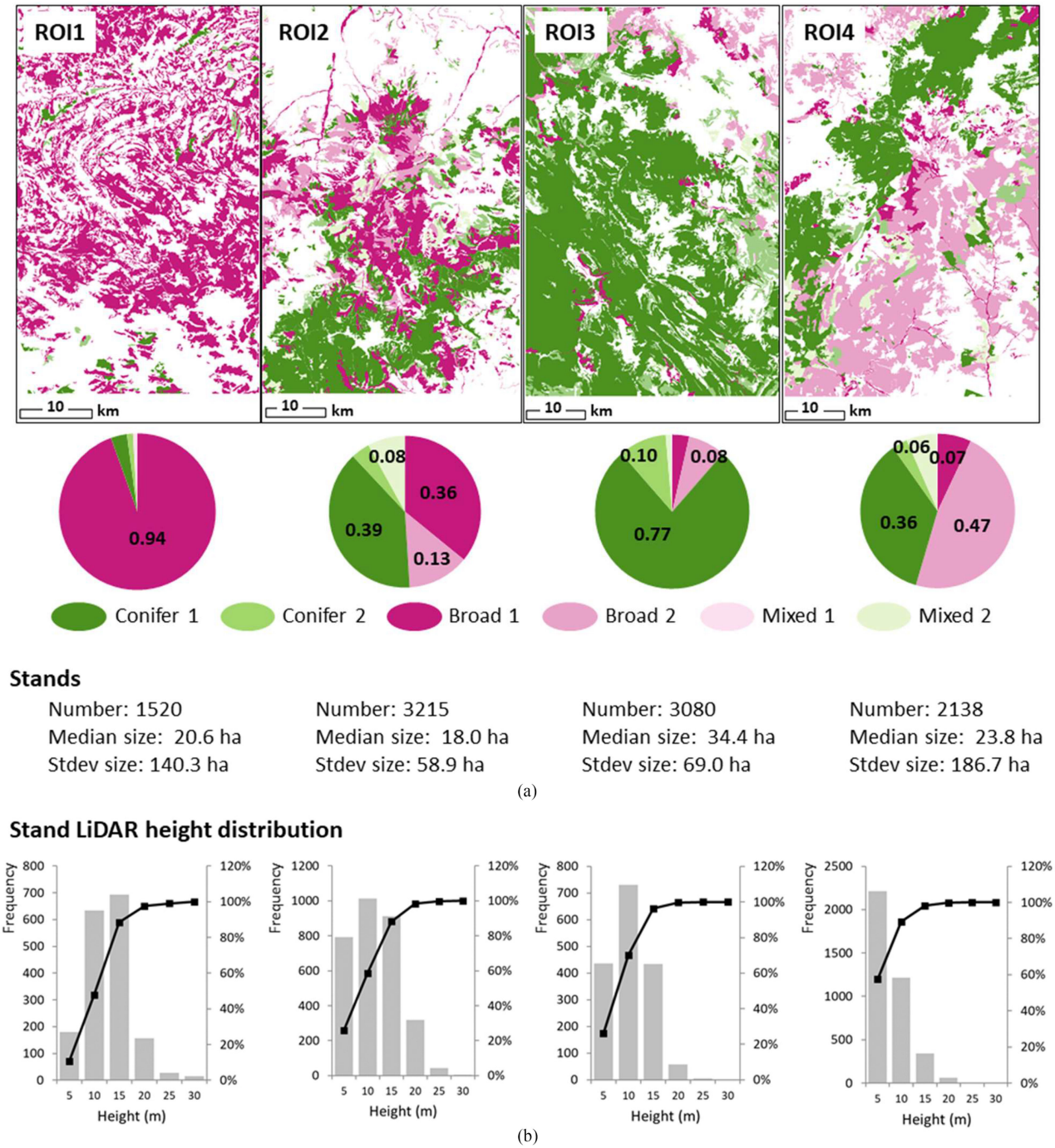

Fig. 2. Characterization of the four ROIs. (a) Forest type proportion and spatial distribution (adapted from MFE50 [35]). (b) Stands composition and LiDAR-derived stand height distribution (PNOA, http://pnoa.ign.es/). The dotted line indicates the cumulative density function.

defined in the Spanish Forest Map version for the year 2012 (MFE50 [35]) were considered a reliable reference database at some stages of our work, such as stratification and accuracy assessment. MFE50 is a country-wide database updated every 3 years, defining areas with the same species composition, and similar density. As ROIs were purposely defined to represent different forest conditions, their stand composition and within height distribution differ [see Fig. 2(a) and (b)]. ROI1 is dominated by temperate broadleaved tree species (Broad 1) and encompasses 1520 stands of 20.6 ha size on average, whereas ROI3 is dominated by coniferous forests (Conifer 1), mainly *Pinus,* and encompasses 3080 stands of 34.4 ha on average. In contrast, ROI2 (3215 stands of 18.0 ha on average) and ROI4 (2138 stands of 23.8 ha on average) are much more heterogeneous and encompass various forest types [see Fig. 2(a)]. The height in more than 90% of the stands in all ROIs is below 20 m. ROI4 is particularly dominated by short heights (only 10% of the stands' height is over 10 m), whereas the other three ROIs are

TABLE II
INDIVIDUAL DATA TAKES OF TDX SELECTED FOR THE FOUR TEST SITES

Area	Date	HoA (m)	Look angle (°)	Kz (rad/m)
ROI1 pair 12	04/07/2012	33.47	45.09	0.19
ROI2 pair 06	28/12/2012	36.58	34.75	0.17
ROI3 pair 02	23/10/2012	32.29	47.74	0.19
ROI4 pair 05	22/12/2012	34.27	34.68	0.18

TABLE III
ACQUISITIONS EMPLOYED IN THE WIDE AREA INVERSION CARRIED OUT OVER THE LARGE ROI2

Area	Date	HoA (m)	Look angle (°)	Kz (rad/m)
ROI2 pair 01	14/12/2011	103.78	46.29	0.06
ROI2 pair 02	05/01/2012	94.37	47.74	0.07
ROI2 pair 03	05/05/2012	28.92	46.72	0.22
ROI2 pair 04	28/12/2012	33.09	34.76	0.19
ROI2 pair 05	28/12/2012	34.78	34.72	0.18
ROI2 pair 06	28/12/2012	36.58	34.75	0.17
ROI2 pair 07	21/12/2011	46.79	32.28	0.13
ROI2 pair 08	13/02/2012	64.42	36.09	0.10
ROI2 pair 09	05/05/2012	29.27	45.75	0.21
ROI2 pair 10	20/12/2011	50.96	36.12	0.12
ROI2 pair 11	20/12/2011	49.33	36.04	0.13
ROI2 pair 12	31/12/2011	45.77	32.12	0.14
ROI2 pair 13	13/02/2012	62.65	36.06	0.10
ROI2 pair 14	31/12/2011	67.35	33.67	0.09
ROI2 pair 15	07/02/2012	98.97	46.30	0.07
ROI2 pair 16	07/02/2012	99.07	45.21	0.06
ROI2 pair 17	05/01/2012	74.97	47.66	0.08
ROI2 pair 18	29/06/2012	30.98	45.16	0.20
ROI2 pair 19	14/12/2011	76.00	46.17	0.08
ROI2 pair 20	29/06/2012	33.78	45.06	0.19

more balanced, with a majority of stand heights between 5 and 20 m [see Fig. 2(b)]. ROIs show also a wide range of topography cases, from flat areas to very mountainous regions.

B. TDX Data

The input data for forest height retrieval consist of TDX products in Coregistered Single-look Slant-range Complex (CoSSC) format. These products contain a pair of images that are already coregistered and, therefore, enable a direct generation of interferograms. Single-polarization (at HH channel) data were chosen for this study because they constitute the most frequent acquisition mode, hence ensuring the largest possible spatial coverage. In all cases, the acquisitions were obtained from ascending passes of the satellites.

The spatial resolution of the original CoSSC images is 3.3 m in azimuth and 2.4–3.4 m in ground range, where it is noted that the resolution in the ground range is not the same for all products due to differences in the incidence angle (or antenna beam). The pixel spacing is around 2–2.5 m in both directions.

Table II lists the details of four data takes (i.e., image pairs) employed to compare the retrieval results over different ROIs. In this case, all present a similar height of ambiguity (HoA) (between 32.3 and 36.6 m). The selection of these HoA values, smaller than in other works with TDX data, is justified in Section II-D and discussed later in the manuscript. In addition, Table III describes all the image pairs considered over ROI2, which will be also employed in Section III to analyze the influence of slope, forest type, and baseline on height retrieval performance.

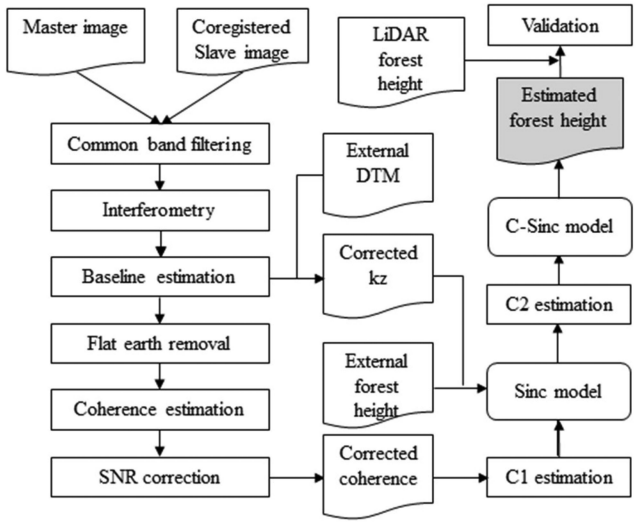

Fig. 3. Flowchart of forest height estimation with the C-sinc model.

C. LiDAR Data

The Spanish National Territory Observation Program (Plan Nacional de Observación del Territorio) [36] supplies remote sensing data covering the entire country, including low-density airborne LiDAR data (0.5 point $\times$ m^{-2}) acquired between 2009 and 2015, with the intention to have repeated LiDAR data coverage of the country every six years. A second LiDAR acquisition (1–14 point $\times$ m^{-2}) is already available in some areas, promising important opportunities to assist forest monitoring. We downloaded LiDAR data contemporary with the TDX imagery from the IGN website portal[1] for validation of TDX-derived heights.

D. Methodology

The overall methodology employed for processing the data, for estimating heights, and for validation is illustrated in Fig. 3.

The TDX system can simultaneously acquire two SAR images used for interferometry. Assuming that the two SAR images are S_1 and S_2, interferometry is performed by

$$\gamma = \frac{\langle S_1 \cdot S_2{}^* \rangle}{\sqrt{\langle |S_1|^2 \rangle \cdot \langle |S_2|^2 \rangle}} \quad (1)$$

where γ is the complex interferometric coherence, composed of interferometric phase φ and coherence amplitude $|\gamma|$. The brackets in (1) denote spatial averaging, which has been carried out using a 9×9 boxcar filter. Therefore, the resulting spatial resolution of the interferograms is around 20 m. In the final geocoding step, a pixel size of 10 m is employed. Although the interferometric coherence is free from the impact of the temporal decorrelation in the case of TDX, it is decreased by decorrelation sources related to volume scattering, spatial baseline, signal processing, thermal noise, and quantization of the SAR data [38]. Among these factors, the volume decorrelation γ_v is related to forest vertical structure and is key to retrieve forest

[1][Online]. Available: https://centrodedescargas.cnig.es/

parameters. The rest of the decorrelations sources are canceled or minimized by known specific strategies [39] and, as a result, volume decorrelation is then measured directly as the complex interferometric coherence γ.

To retrieve forest height from γ_v, a forward model of the scene is needed. The RVoG model has been widely used for modeling the volume decorrelation, which simplifies the forest scene as a two-layer vertical arrangement consisting of a ground surface and a vegetation layer. The RVoG model provides a simple expression of the volume coherence as [40]

$$\gamma_v = \exp(i\varphi_0)\frac{\gamma_{v0}+m}{1+m} \tag{2}$$

where φ_0 is the ground phase, which is linked to subcanopy topography; m denotes the ground-to-volume backscatter ratio; and γ_{v0} is the volume decorrelation produced by the vegetation volume alone, which can be expressed as [23], [41]

$$\gamma_{v0} = \frac{\int_0^{h_v} \exp\left(\frac{2\sigma z}{\cos\theta}\right)\exp(ik_z z)\,dz}{\int_0^{h_v} \exp\left(\frac{2\sigma z}{\cos\theta}\right)dz} \tag{3}$$

where h_v is the forest height; σ is the extinction, which is a function of density of forest scatterers and their dielectric constant; θ is the incidence angle; and k_z is the vertical wavenumber, which determines the sensitivity of the InSAR system to the forest height.

Due to the number of model parameters involved, fully polarimetric SAR data are required to make the RVoG model invertible. However, since the main operational acquisition mode of the TDX system is in single polarization, the inversion constitutes an under-estimated problem. Two strategies have been proposed to address this issue: providing auxiliary data (e.g., DTM to work directly with the interferometric phases), or simplification of the RVoG model. The second option has been widely adopted in forest studies with TDX. Assuming that there is no response from the ground ($m = 0$) and the extinction is null ($\sigma = 0$), the measured volume decorrelation in (2) can be simplified as [25]

$$|\gamma_{v\_\mathrm{sinc}}| = \mathrm{sinc}\left(\pi\frac{h_v}{\mathrm{HoA}}\right) \tag{4}$$

where HoA is the height of ambiguity (HoA $= 2\pi/k_z$). As a result, the RVoG model is simplified as a sinc function, defined as $\sin(x)/x$. However, in practice, the sinc model in (4) cannot provide reliable forest height estimation because the above two assumptions are not held in many cases. To solve partially this limitation, the so-called C-sinc model was first proposed by Olesk *et al.* in [25]

$$|\gamma_{v\_C\mathrm{sinc}}| = C_1\,\mathrm{sinc}\left(C_2\pi\frac{h_v}{\mathrm{HoA}}\right) \tag{5}$$

where C_1 and C_2 are empirical parameters. The core idea of the C-sinc model is that, as shown in Fig. 4, by adjusting C_1 and C_2, the model can globally fit the observed coherence values so that the effect of the mismatch error between the coherence and the sinc model on forest height estimation can be reduced.

At this point, it is important to discuss the influence of the hypotheses considered in the direct model. The assumptions of

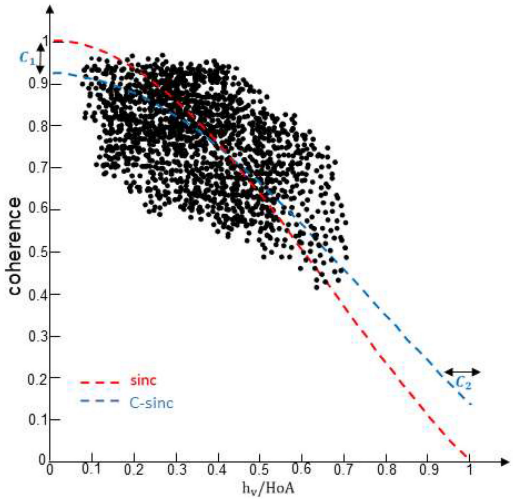

Fig. 4. Diagram of the sinc and C-sinc models.

the absence of ground contribution ($m = 0$) and rectangular volume reflectivity profile ($\sigma = 0$) lead to the pure sinc model relating coherence and forest height (4). This over-simplification is adopted to make the model invertible. However, one should always expect some radar response from the ground, which entails $m > 0$, and, therefore, a mismatch between the model and the data. This mismatch could be alleviated by previous knowledge of the value of the ground-to-volume ratio (m), and also by adopting a more realistic vertical reflectivity profile. Initially, a wide set of tests with different values of m and different profiles was carried out, but the best parameter values (i.e., the ones providing the best fit between data and model) were found to vary strongly as a function of the position in the scene. Consequently, a rule to apply a particular combination of m and profile, either to the whole scene or with a varying pattern, was not found.

An alternative way to alleviate the mismatch between the data and the sinc model consists in modifying the sinc model with (two) empirical constants, as it is done in the C-sinc model employed here [25]. In this way, instead of modifying the direct model by a new vertical reflectivity profile or by imposing a new value of the ground-to-volume ratio, the inversion model is modified by calibrating the C-sinc model. With this strategy, the focus of the methodology is on the height inversion (which at the end is the final objective of this work) instead of on the physical modeling of the radar response.

As a result of this strategy, the reflectivity profile that would correspond to the C-sinc model, which is empirically calibrated to fit the data, is not known. However, the lack of knowledge of the profile embedded in the model would be an issue only if the objective were to derive some physical variable related to the vertical structure, e.g., biomass. From the point of view of height estimation, in practical terms, the real profile is not required, provided that the estimation accuracy is good.

It is also important to mention that the vertical wavenumber k_z, and hence the HoA, depends on the local incidence angle, which in turn depends on the look angle of the satellites and the local slope. Consequently, the local slope at the entire scene

must be known (usually derived from an auxiliary DTM) to work properly with the sinc and the C-sinc models.

The HoA provides information about the sensitivity of the coherence to height changes. In [26], the performance of the forest height estimation by means of TDX data was found to be optimum in the interval of forest heights between HoA/3 and HoA. This means that when the forest height is much smaller than HoA, the system is not sensitive, and the height cannot be estimated accurately. One key aspect to take into account in our study is the short trees forming the Mediterranean forests [see Fig. 2(b)], in contrast with temperate and tropical forests. The vast majority of forest height values are below 15 m in all test sites, with maximum percentages of trees between 2 and 10 m height. This means that the interferometer is required to provide sensitivity to variations in vegetation height within that interval, and this can be achieved only with large baselines (i.e., large values of k_z), which correspond to small values of HoA. This is the reason why relatively small values of HoA were selected (when available).

The determination of C_1 and C_2 in (5) is necessary to establish the relationship between forest height and coherence. According to (4), when the forest height is zero, the coherence should be 1. However, due to residual processing errors and noncompensated decorrelation sources, the coherence corresponding to zero forest height is less than 1. An empirical value of 0.93 was suggested in [25] for the scaling constant $C_1$to address this issue. In this work, the method used by Chen *et al.* [26] is adopted to determine C_1, which represents the residual processing error. Chen's method starts by generating the full spectrum of coherence values, from dense forest to clear cut. The cumulative density of coherence values is obtained, and the offset compensation is selected between the coherence saturation value in this distribution and unity as C_1.

Regarding C_2, it can be determined according to a priori information about the mean scattering center height [25] or calculated by fitting coherence values [26]. In the second case, when known forest height values are input to the model, C_2 is chosen to best fit the model to the coherence values. However, in mountainous forest areas, the effect of topographic slope should be carefully considered, as it can reduce and distort the interferometric coherence. In such a case, the slope-induced decorrelation will distort the relationship between the interferometric coherence and the forest height, making the fitting method that directly fits between observed coherence and C-sinc model become unstable and biased. Although C_1 can absorb the decorrelation caused by residual processing errors, it does not compensate the effect of topographic slopes, which will just be partially absorbed by C_2 during the fitting process. As a result, the obtained C-sinc model cannot perfectly convert the interferometric coherence to forest height. Thereby, we here suggest not using the C-sinc function to fit the observed interferometric coherence as described in [26], but to find a C-sinc function (i.e., the C_2value), which predicted forest heights show the highest accuracy, that is, we search the optimal C_2, by minimizing the corresponding residual forest height inversion error. In such a way, to some extent, the C-sinc model obtained not only takes into account the mismatch between sinc-model assumption and real forest scenario but also avoids the effect of slope-induced decorrelation on forest height estimation.

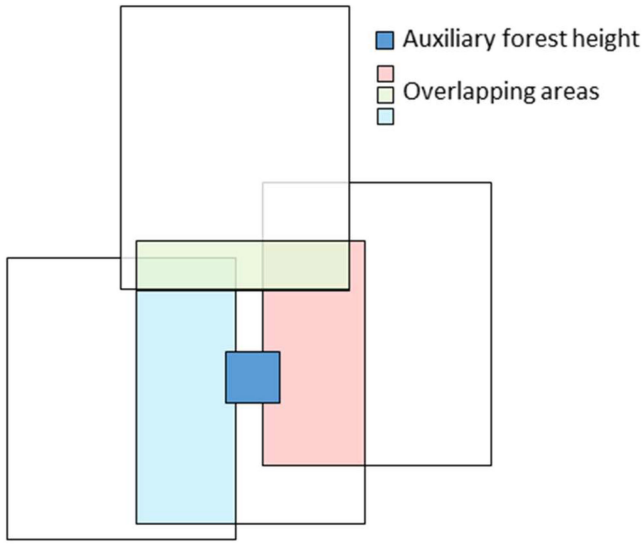

Fig. 5. Schematic representation of the process implemented for large-scale forest height estimation including auxiliary heights at small scale.

To identify the unknown parameters in the C-sinc model, a small amount of auxiliary forest heights is needed to perform the training. However, in practice, it is not possible to provide auxiliary forest heights for every footprint of TDX InSAR data, making it difficult to estimate forest height with the C-sinc model in large areas. In this work, we developed an approach for large-scale forest height estimation, as shown in Fig. 5. The core idea of the proposed method is that only a small patch of LiDAR forest height is selected as the initial central patch to invert forest height for the first TDX image, with the most accurate C-sinc model parameters obtained. The model parameters used in the inversion of the remaining images are trained based on the overlapping area with the previous scene image as "reference" data, which means the model parameters are transferred from the control image (usually the central image) to the rest of the images (the edge of the large ROI). To be more specific: first, the interferometric pair with the largest coverage of auxiliary forest height data is selected to generate forest height with the C-sinc model with the procedure shown in Fig. 3. Then, the next interferometric pair with largest overlap with the last estimated forest height map is selected for C-sinc model inversion, where the model parameters are determined through the overlapping areas, that is, the model parameters are estimated using the inversion result from the last image (overlapping area), being assumed as "reference" data. In such a way, we could continue to look for the subsequent interferometric pair with the largest coverage of the previous TDX forest height map and perform such extension until all interferometric pairs are processed. Therefore, the precision of the C-sinc model parameters gradually degrades from the first to the last pair through the continuous transfer by overlapping regions. For this reason, as for the region covered

by more than one interferometric pairs, the earliest inversion results in overlapping regions (from all possible estimates) are selected as final output estimates.

The influence of topographic slope, forest type, and image pair baseline on the retrieval of forest heights from TDX coherence was analyzed with tests controlling the other factors.

E. Comparison With Reference LiDAR Height

Validation of the height outcomes was done with the contemporaneous LiDAR data ($\pm$ 2 years) available over the entire area.

Previously, the fitting of the C-sinc model parameters is carried out using the LiDAR reference data at pixel level to preserve the fine spatial details and local slopes available. Since C_2 plays an important role in absorbing residual errors induced by the terrain slope effects and mismatches between the sinc model and InSAR observations, if we perform this step at the stand level, the slopes would be wrongly averaged so that the estimated C_2 could not take into account the terrain effect, biasing the final forest height conversion. On the other hand, when performing the validation, stand-level inventory can meet some of the users' and managers' needs, such as carbon and diversity reporting, etc.

Therefore, height retrieval results are presented in three ways: maps, scatter plots, and tables with validation scores. Maps are computed at a pixel level to show the spatial variability of the results, whereas all quantitative validation measurements (scatter plots and validation scores) are computed at the stand level, for which the forest stand is considered as the homogeneous spatial unit defined by the MFE. The two average values are used for generating the validation scatter plots and for computing the validation indices: root-mean-square error (RMSE) and coefficient of determination (R^2).

III. Results

A. Overview of the Correspondence Between Model and Data

Before analyzing the forest height inversion results, we inspect here the input data (i.e., absolute value of the coherence) and its sensitivity to forest height, for which individual scenes are selected at the four test sites. The main parameters of the four scenes are shown in Table II. It is important to note that the HoA for zero slope of the four scenes is very similar (32–37 m), so a relative comparison among ROIs is also possible.

This inspection is carried out by representing in Fig. 6 the measured coherence (already corrected as it is used for inversion, as described in Section II) as a function of the corresponding LiDAR forest height (normalized by HoA). This type of representation, which has been used by other authors in the past [19], [25], [37], is useful to check the correspondence between direct model and data.

Fig. 6 shows that the data do not follow the pure sinc model, so the C-sinc modeling described in Section II is required to provide good height estimates in the retrieval. A second obvious comment from Fig. 6 is that the four ROIs are characterized by point clouds with different shapes, i.e., they exhibit different

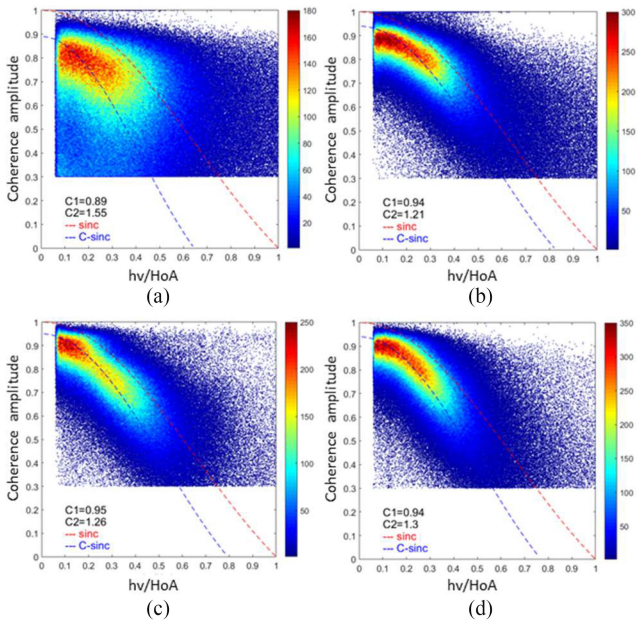

Fig. 6. Plots of coherence versus LiDAR forest height/HoA. (a) ROI1. (b) ROI2. (c) ROI3. (d) ROI4. The original sinc model is represented with a red dashed line, whereas the C-sinc model is plotted with a blue dashed line. Coherences below 0.3 are not shown.

distributions of data, reflecting their diversity of forest types and topographical features. In all cases, however, there is a low percentage of points (less than 10%) with forest height greater than HoA/2. This means that, as expected, these scenes are characterized by short trees typical of Mediterranean regions, which are much shorter than temperate or tropical forests previously studied in the literature.

In detail, ROI1, which is the site with tallest trees (dominated by Broad 1 class) and with the most abrupt topography, exhibits a very wide cloud of points in Fig. 6(a). Therefore, there is a big proportion of points that depart from the fitted model. For instance, there are many points with forest height between 0.1 HoA and 0.3 HoA, where coherence values are below 0.7. Notably, the area with the highest density of points at ROI1 is wide and arranged rather horizontally. This means that the measured coherence does not change clearly with forest height, i.e., there is no sensitivity to forest height at that interval, which is probably caused by the presence of variable and strong slopes. This leads, in parallel, to a mismatch between data and model. The assumptions taken in the model to make it invertible (null extinction and null ground response) are the most plausible causes of the mismatch.

The other three ROIs present a much better correspondence between the data and the model [see Fig. 6(b)–(d)] since coherence decreases when forest height increases, following the sinc-type function used for the model. In the case of ROI3, shown in Fig. 6(c), most data points are concentrated in a small region in this representation, i.e., the main range of forest heights is very narrow (dominated by short trees with heights below 0.15 HoA), whereas in ROI2 and ROI4 there is a wider range of points following the C-sinc model pattern.

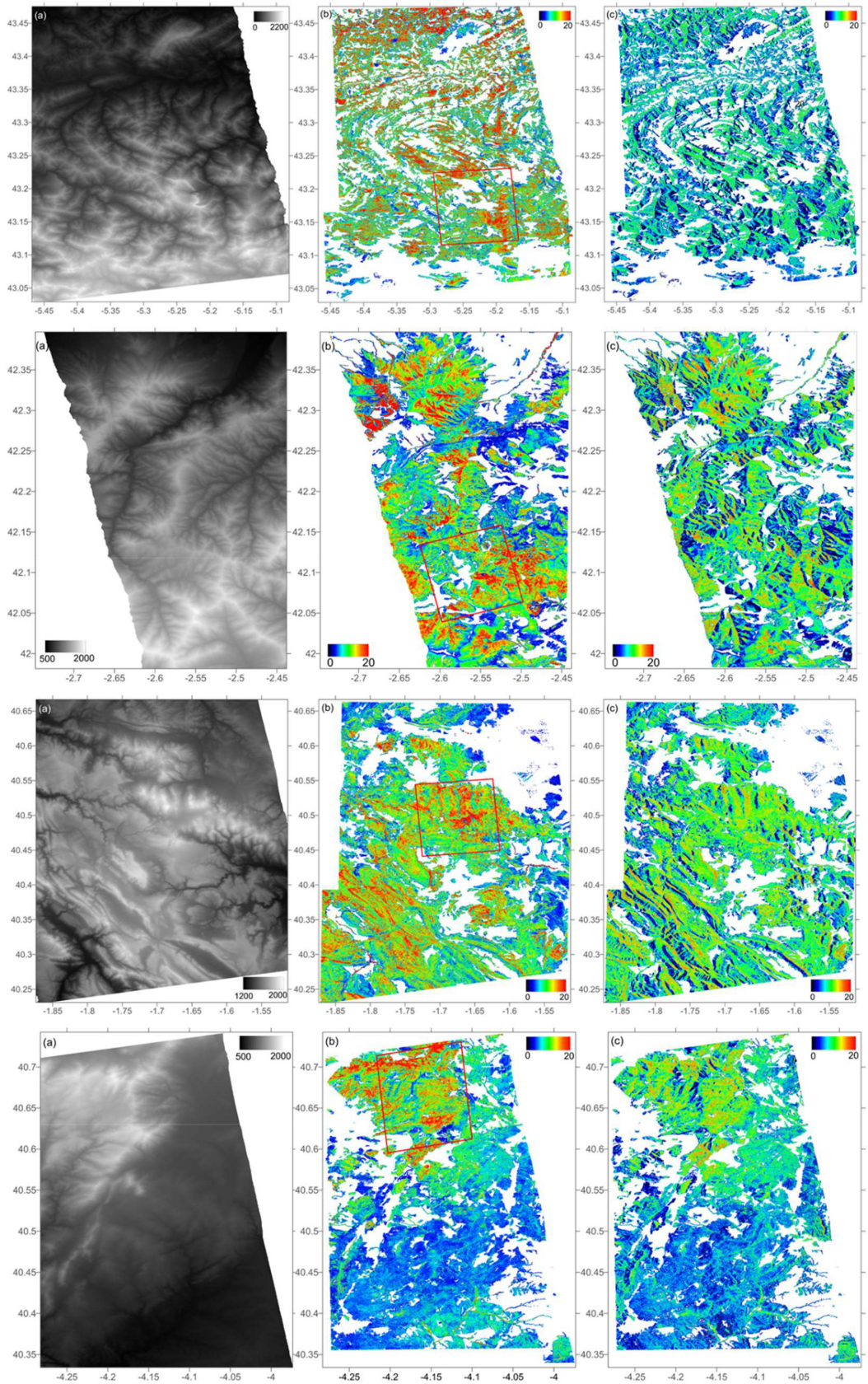

Fig. 7. Inversion results over a scene in each ROI. (a) LiDAR DTM. (b) LiDAR forest height. (c) TDX-retrieved forest height. The red rectangle in (b) represents the area with LiDAR data used for the C-sinc model calibration. Top to bottom: ROI1, ROI2, ROI3, and ROI4.

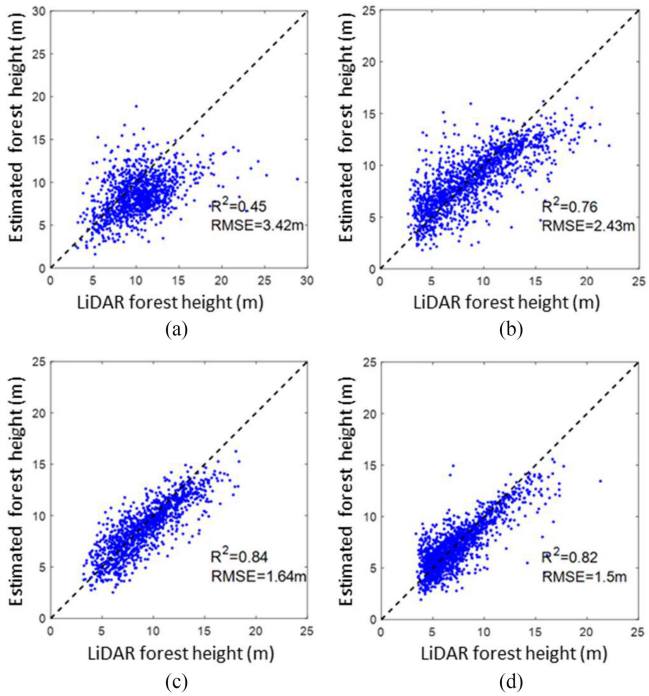

Fig. 8. Scatter plots of retrieved height versus true (LiDAR) height, computed using forest stands over the scenes defined in Table I. (a) ROI1. (b) ROI2. (c) ROI3. (d) ROI4.

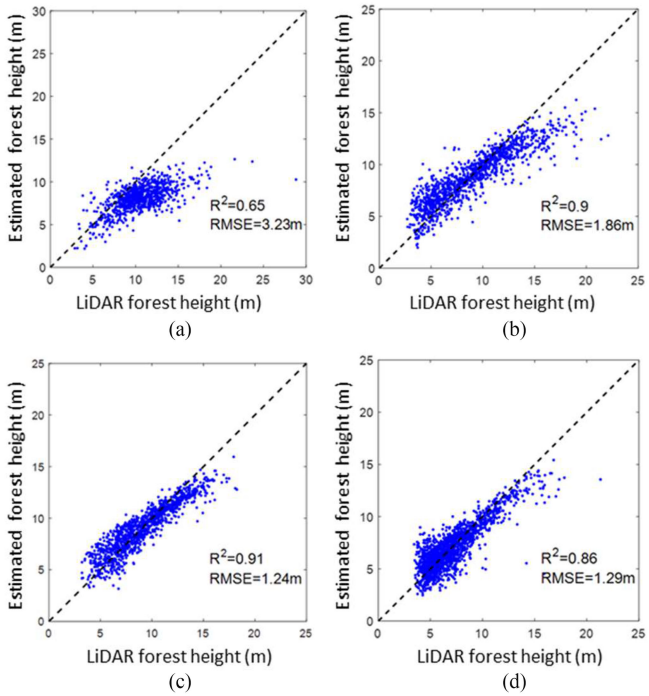

Fig. 9. Scatter plots of retrieved height versus true (LiDAR) height, computed using forest stands over areas with slopes between –10° and 10°. (a) ROI1 (819 stands). (b) ROI2 (1181 stands). (c) ROI3 (1144 stands). (d) ROI4 (1766 stands).

Regarding the constants C_1 and C_2 in the C-sinc model, which are calibrated independently at each ROI, there is not much difference among ROIs. The C_1 constant ranges from 0.89 to 0.95, whereas C_2 goes from 1.21 to 1.55.

B. Retrieved Heights At the Four Test Sites

Fig. 7 shows the spatial distribution of the height retrieval results with a pixel size of 10 m and obtained in the same four selected scenes inspected in the previous section. The topography information (DTM) and the LiDAR forest height are also shown for comparison and interpretation.

In all cases, the spatial pattern of the retrieved heights resembles the LiDAR heights, confirming the mapping ability of the technique applied in these scenarios. However, one can easily appreciate that the most extreme forest heights present in these regions (LiDAR height close to 20 m, represented in red color) are underestimated in the TDX-derived heights. Regarding the heights between 2 and 15 m, there is a quite clear visual correspondence between the LiDAR and TDX height maps.

The scatter plots computed for validation at the four scenes are shown in Fig. 8, in which the R^2 coefficient and the RMSE obtained from the comparison of LiDAR heights and TDX retrieved values are also included. We observe poor correlation at ROI1 ($R^2 = 0.45$) and moderate to high correlations at the other three ROIs (R^2 from 0.76 to 0.84). Moreover, the RMSE ranges between 1.5 m for ROI4 to 3.42 m for ROI1. The scatter plots are obtained by comparing the average heights at the MFE stand level. Due to this strategy, there are only a few points with heights over 15 m. In all ROIs, there is an apparent underestimation of the TDX derived heights, which is clearer for the tallest forest stands, in agreement with the height maps shown in Fig. 7.

C. Influence of Slope

In order to identify the potential influence of the local slope in the results presented in the previous sections, we examined the datasets in locations with slope below 10°, i.e., areas of flat or gentle topography. The C-sinc model was fitted again and the height inversion carried out with the new values. The resulting validation scatter plots are shown in Fig. 9.

Comparing Fig. 9 with Fig. 8, there is an improvement at all ROIs (0.04–0.20 in R^2), and the RMSE is 0.2 to 0.6 m lower than with all slopes, reaching the best value (1.24 m) at ROI3. At ROI1 the improvement is much clearer when we restrict the inversion to low slopes. The coefficient of determination achieves 0.65, whereas the RMSE is now 3.23 m, around 0.2 m lower than with all slopes (3.42 m). As deduced from the shape of the point clouds in the scatter plots in Fig. 9, we can conclude that the performance of this methodology will be much better at ROI2, ROI3, and ROI4 than at ROI1.

D. Influence of Forest Type

In addition to the local topography, the type of forest is expected to affect the performance of the forest height retrieval from the TDX data. The structural features of the forest types present in Spain are quite diverse, and they may have a strong influence on the validity of the model employed for the coherences and the assumptions taken for the inversion. In order to check

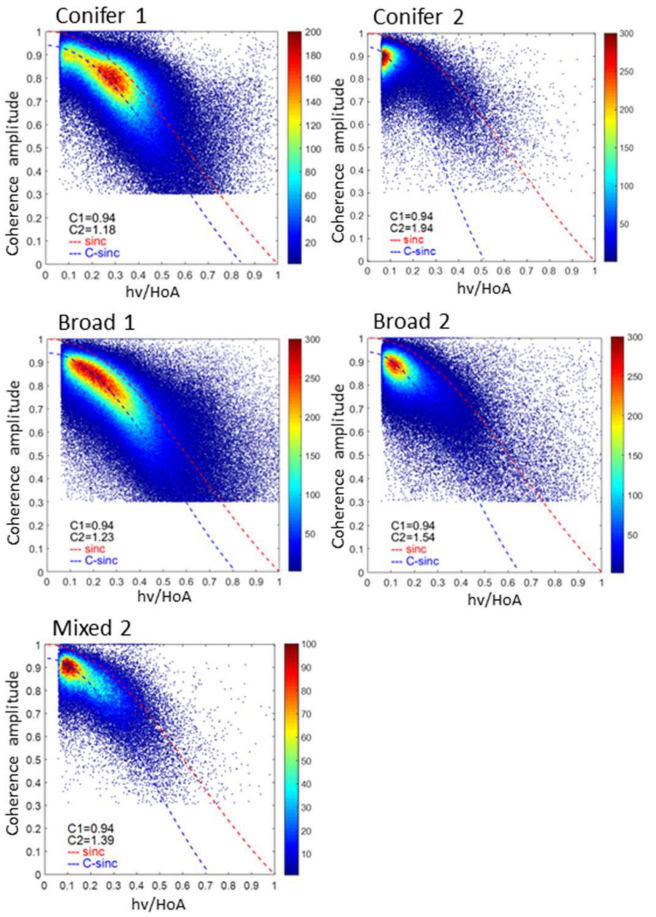

Fig. 10. C-sinc model fitting for different forest types at ROI2, considering only slopes between ±10°. *N* denotes the number of samples; C_1 represents the systematic correction (scaling constant); C_2 denotes the empirical parameter in C-sinc function. The number of Mixed 1 samples in this area is so low that the model fitting is meaningless and not shown.

TABLE IV
VALIDATION RESULTS OBTAINED FOR EACH FOREST TYPE (SLOPE ±10° ONLY)

Forest type	RMSE (m)	R^2
Conifer 1	1.92	0.89
Conifer 2	2.52	0.88
Broad 1	1.67	0.90
Broad 2	2.08	0.84
Mixed 2	1.98	0.89

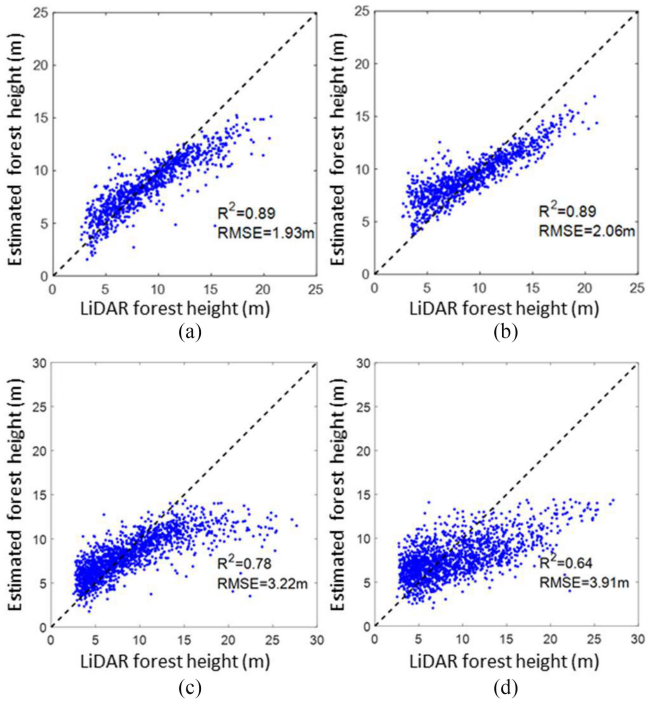

Fig. 11. Scatter plots of retrieved height versus true (LIDAR) height, computed using forest stands over areas with slopes between –10° and 10° at ROI2. (a) Pair 06. (b) Pair 14. (c) Pair 09. (d) Pair 19 (see Table III for details).

that influence, the plots of measured coherence as a function of LiDAR height (used also in Fig. 6) are shown in Fig. 10 for the five forest types present in ROI2. In this case, the slopes are limited to +/–10°, as it was done in Section III-C, to isolate the effect of forest type from the effect of slope. The C-sinc model has been fitted to each forest type independently, and both the model curves and the fitted parameters (C_1 and C_2) are shown in Fig. 10.

Forest types named Broad 1 and Conifer 1 show the most dynamic range of values. In both cases, the data follow the C-sinc model well, particularly in the case of Broad 1. The other three forest types (Conifer 2, Broad 2, and Mixed 2) are dominated by very short trees, but in general there is also agreement with the model, i.e., coherence decreases as forest height increases. However, constant C_2 in the fitted model changes notably for each forest type, from 1.18 at Conifer 1 to 1.94 at Conifer 2. This indicates that the retrieval performance could be improved if the model was calibrated independently by forest type.

Following this strategy, the resulting validation scores obtained for each forest type at ROI2 are presented in Table IV. The coefficients of determination range from 0.84 to 0.90, providing RMSE values between 1.67 and 2.52 m. Notably, with respect to the scores found in Section III-C at the same ROI when no separation of forest types is considered ($R^2 = 0.90$ and RMSE = 1.86 m), there is only improvement in class Broad 1, whose new RMSE is 1.67 m.

E. Influence of Baseline

The scenes are observed by TDX under different incidence angles and using a range of baselines (spatial separation between the two satellites). Baseline is a system parameter that affects importantly the sensitivity of the interferometric products to height variations in the scene. The HoA is inversely proportional to the baseline, so its value changes the expected range of coherences for the same interval of forest height [see (4) and (5)].

Fig. 11 shows the scatter plots comparing LiDAR forest height and TDX-derived height over the same area in ROI2 but using four different data takes (numbered as pairs 06, 14, 09, and 19 in Table III), characterized by HoA equal to 34, 70, 29, and 76 m, respectively. Pairs 06 and 14 (top row) and pairs 09 and 19 (bottom row) correspond to slightly different geographical areas

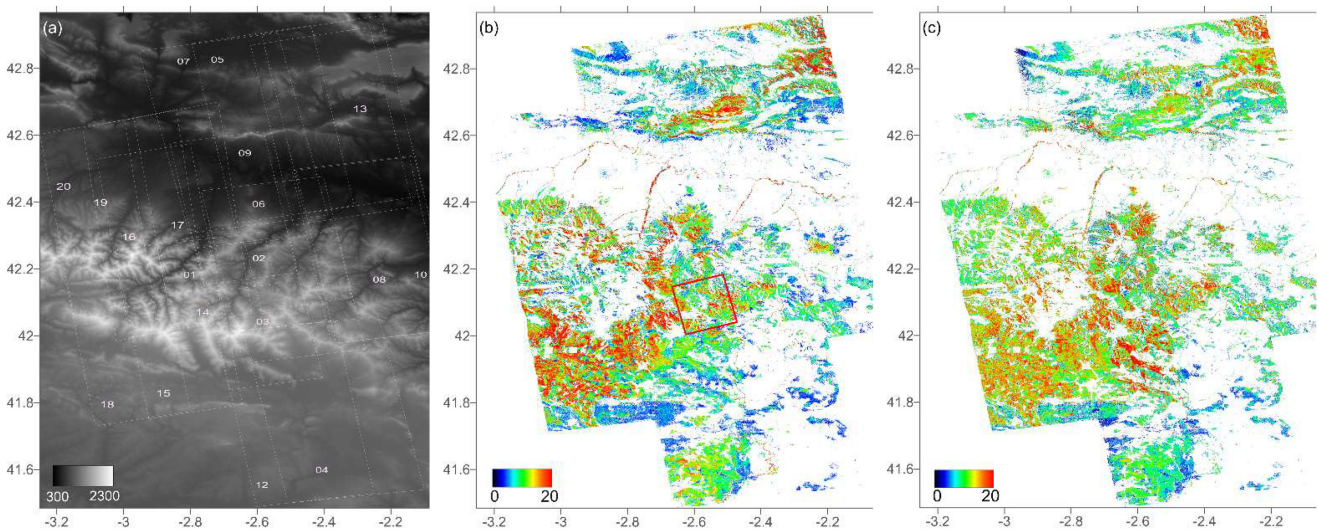

Fig. 12. Inversion results over the entire ROI2. (a) DTM with image pairs footprints. (b) LiDAR forest height. (c) TDX forest height. The red rectangle in (b) represents the location of the LiDAR data used for calibration.

within ROI2. Pairs 06 and 14 provide very similar validation scores despite their different HoA, whereas pair 19 presents values of R^2 and RMSE clearly worse than pair 09 (i.e., RMSE is 0.7 m higher for the longest HoA).

F. Wide Area Results

Finally, since the goal of this project is to generate a forest height map of the entire country, a strategy is required to process and combine groups of TDX acquisitions to provide a complete map. This section presents the first large-scale map generated in the project, which covers the enlarged ROI2, with an area of 103 $\times$ 179 km. To generate this map, a set of 20 acquisitions, listed in Table III, was exploited. Some image pairs are characterized by relatively large values of HoA, and do not meet the ideal HoA requirements of the short trees present (see Section III-E). However, there were no acquisitions with smaller HoA values in the same locations and these pairs are necessary to completely cover the large ROI considered. The results obtained are shown in Fig. 12, in which the DTM and the footprints of all acquisitions are also displayed.

In general, the map with the TDX-derived heights resembles the map of LiDAR forest heights, although there is a clear underestimation in some areas, like the SW and NE regions of the site. It is worth noting that, despite the height values were retrieved from different acquisitions, the TDX height map does not show any discontinuity or jump in height values.

Fig. 13 shows the validation scatter plot corresponding to this wide area result. As it was already stated, there is a clear underestimation of the tallest trees' heights (especially over 15 m), and the resulting scores are worse than for the single scene results shown in Section III-B. The RMSE increases from 2.43 to 3.33 m, and R^2 decreases from 0.76 to 0.61 (see Fig. 8 for comparison). This degraded performance, compared with the single scene case, was expected. As described in Section II-D, the LiDAR data is employed just for calibration of the TDX

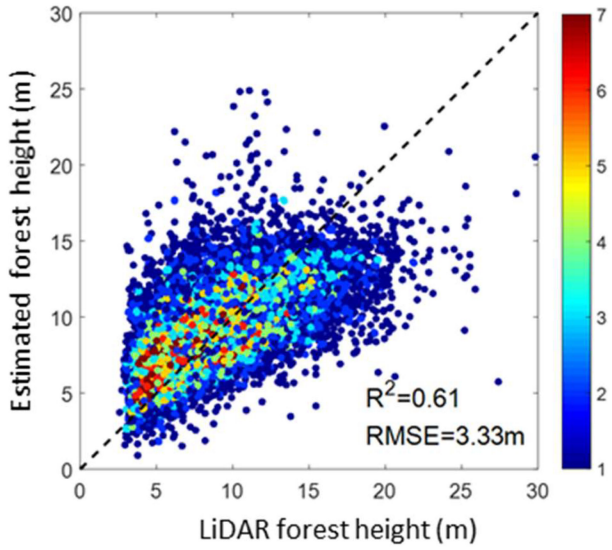

Fig. 13. Scatter plots of retrieved height versus true (LIDAR) height, computed using forest stands over the whole ROI2.

heights in its covering scene, whereas the rest of TDX scenes are calibrated with TDX-derived heights from the overlapping zones.

In addition, no separation by slope or forest type was applied, which means that this result is subject to improvement once a stratification framework (by classes of slope and forest type) is devised and applied.

IV. Discussion

It is important to understand how radar signal and modeling varies among different types of forests (tropical, boreal, temperate, Mediterranean) [5]. In this work, we explored for the first time the potential application of TDX interferometry

for the estimation of canopy height in Mediterranean forests. Two aspects make this application different from previous work in other biomes: the location of forests in very rugged terrain in mountain areas, and the relatively short average height of forest stands. Furthermore, aiming to produce a large-scale map of forest heights, data availability can become a challenge. Therefore, this work was focused first on analyzing the overall performance of the approach, following a known method (the C-sinc model) for height retrieval. Then, the influence of specific scene features (slope and forest type) and system parameters (interferometric baseline) was evaluated.

Compared with LiDAR heights, the retrieved height values were in general underestimated, and more notably for trees taller than 15 m. A possible reason is that the proportion of trees shorter than 10 m is very high, so they have a strong impact on the C-sinc model calibration. In addition, the fitted model, although better than the sinc model, follows the measured data only partially. Therefore, another analytical function (e.g., a polynomial or another function with more parameters) with a better fit to the data over the whole dynamic range of forest height should be considered, especially to avoid the mentioned underestimation for the largest height values.

As a more flexible alternative, the use of machine learning is expected to overcome this limitation and to provide better estimates in a wider range of forest heights. For instance, convolutional neural networks have been used recently for the forest height retrieval from polarimetric SAR interferometry data [43].

Another important aspect to be studied in the future is the amount of wave penetration achieved in the Mediterranean forests present in Spain. If penetration is too low, the interferometric measurements are not sensitive to the whole vegetation volume, which leads to wrong height estimates. In general, the use of X-band data is influenced by a limited penetration in forest scenarios and, consequently, an ancillary ground DTM is required to provide accurate height estimates. Owing to both the short height of the trees and the low tree density that characterizes some Mediterranean forests, we expect that the penetration is larger than in other scenarios (e.g., tropical or temperate forests). Although this could be concluded from the good height estimation accuracy obtained so far, this specific aspect needs to be corroborated experimentally. In addition, provided that a LiDAR-based subcanopy DTM is available for the entire Spain, the forest height inversion could be approached in the complex domain. This would contribute with an additional structural parameter that can be used to adapt the model across wide ranges of slope and forest types.

Attending to the results found in this study, the slope in the scene influences notably the performance of the forest height inversion. Over flat areas, i.e., with slopes below 10°, the coherence values exhibit a better sensitivity to forest height. Consequently, despite the assumptions taken in the model employed for inversion (null extinction and null response from the ground), for flat areas the height estimates are considered satisfactory (R^2 over 0.85 in three ROIs, with RMSE below 1.3 m in two of them), without forest-type stratification. In contrast, the presence of high slopes breaks a homogeneous relationship between coherence and height and, as a result, the estimation performs poorly if this is not considered. A potential solution, to be explored in future works, consists of the stratification per slope prior to calibration of the C-sinc model constants (i.e., fitting different constants for different slope intervals). Regarding forest type, an analysis was conducted over one of the ROIs (ROI2), in which five classes are present. Results did not improve when the model was calibrated differently for each forest type. An improved stratification by forest type, with a more specific consideration of stand density, should be considered in future efforts. Likewise, our validation of retrieved heights by spatial units with a more homogeneous height distribution may provide more reliable values of accuracy and more specifically reveal the relevant factors affecting the retrieval performance. In this work, we relied on a nationwide spatial database (MFE), which does not specifically consider height as a criterion to define forest areas, resulting in large stands with a variable within heights. The aggregation of height to average values may be confounding the real accuracy that could be reached by the estimation method. Although valuable reference units with ecological meaning, the MFE stands are too large and heterogeneous if a sylvicultural use is envisaged. These stands could be further segmented into smaller and more height-homogeneous units to employ as reference. Therefore, the main conclusion of our first analysis of ground factors is that slope seems to be a more determinant factor than forest type, affecting the coherence data provided by TDX and, therefore, the application of the retrieval algorithm should be carried out with a previous separation of slope values for model calibration and inversion.

As for the influence of the interferometric baseline, the short trees in this geographical area require the exploitation of interferograms characterized by short HoA values to ensure enough sensitivity. For the same ROI, it was found in some cases that using HoA values around 30 m performed better than HoA values around 70 m. It is important to clarify that this preference for short HoA is specific of this geographical region and is a direct consequence of the short trees present. In other geographical areas (e.g., in tropical or temperate forests) characterized by taller trees, these small HoA values should not be employed because they would lead to ambiguities (wherever $h_v >$ HoA), so larger HoA values are required [42]. In our study region, with the Mediterranean forest, HoA needs to be accounted for when selecting the working interferogram if more than one is available.

Finally, large-area mapping of forest heights is always a challenge, achieving higher accuracy locally, where the model parameters are controlled. In [42], a height map of boreal forest was generated in Sweden, for an area with a similar extension to Spain ($\sim$450 000 km^2) and required more than 500 TDX acquisitions. The mosaicking approach applied by Persson *et al.* [42] resulted in areas with different accuracy in height estimation, due to the variability in acquisition conditions. We designed an approach to spread model fitting parameters from small areas with controlled heights to large areas, based on the previous estimates over overlapping areas. The overall performance degrades progressively as the location moves away from the initial control area. To avoid this issue, a sparse distribution of well-controlled areas should be available. In such a way,

the mentioned degradation would always be under a maximum tolerance.

V. Conclusion

The feasibility of estimating forest height with TDX data in Mediterranean forests has been demonstrated with this work. It has been shown that stratification by forest type and slope is beneficial to improve the accuracy of the retrieved heights, despite the short tree heights found in this geographical region. In addition, a procedure for mapping wide areas using localized reference data for calibration has been tested.

At quantitative level, an overall underestimation in the retrieved heights with respect to LiDAR-derived heights has been found. The simplicity of the physical model exploited, which assumptions are not fulfilled on many occasions, is a clear limitation of the current approach.

Regarding the generation of a large-scale map, eventually over the entire country, the use of distributed reference data will be analyzed. In parallel, the exploitation of GEDI data, which have been successfully combined with TDX data to generate maps of forest height and forest structure [44], [45], is also considered a good alternative for generating consistently accurate maps over large areas.

Acknowledgment

The German Aerospace Center (DLR) provided all the TanDEM-X data under Project OTHER7349.

References

[1] M. Köhl and M. Marchetti, "Objectives and planning of forest inventories," in *Tropical Forestry Handbook*. Berlin, Germany: Springer, 2014, doi: 10.1007/978-3-642-41554-8_70-1.

[2] X. Wu, X. Wand, Y. Wu, X. Xia, and J. Fang, "Forest biomass is strongly shaped by forest height across boreal to tropical forests in China," *J. Plant Ecol.*, vol. 8, no. 6, pp. 559–567, 2005.

[3] R. Valbuena *et al.*, "Standardizing ecosystem morphological traits from 3D information sources," *Trends Ecol. Evol.*, vol. 35, pp. 656–667, 2020, doi: 10.1016/j.tree.2020.03.006.

[4] M. A. Wulder *et al.*, "Lidar sampling for large-area forest characterization: A review," *Remote Sens. Environ.*, vol. 121, pp. 196–209, 2012.

[5] I. H. Woodhouse, E. T. A. Mitchard, M. Brolly, D. Maniatis, and C. M. Ryan, "Radar backscatter is not a 'direct measure' of forest biomass," *Nat. Clim. Change*, vol. 2, pp. 556–557, 2012.

[6] M. Schlund and M. W. J. Davidson, "Aboveground forest biomass estimation combining L- and P-band SAR acquisitions," *Remote Sens.*, vol. 10, 2018, Art. no. 1151.

[7] M. A. Lefsky, "A global forest canopy height map from the moderate resolution imaging spectroradiometer and the geoscience laser altimeter system," *Geophys. Res. Lett.*, vol. 37, 2010, Art. no. L15401.

[8] M. Simard, N. Pinto, J. B. Fisher, and A. Baccini, "Mapping forest canopy height globally with spaceborne lidar," *J. Geophys. Res.*, vol. 116, 2011, Art. no. G04021.

[9] C. Hansen *et al.*, "Mapping tree height distributions in sub-Saharan Africa using Landsat 7 and 8 data," *Remote Sens. Environ.*, vol. 185, pp. 221–232, 2016.

[10] L. I. Duncanson, K. O. Niemann, and M. A. Wulder, "Integration of GLAS and Landsat TM data for aboveground biomass estimation," *Can. J. Remote Sens.*, vol. 36, pp. 129–141, 2010.

[11] D. Lu, "The potential and challenge of remote sensing-based biomass estimation," *Int. J. Remote Sens.*, vol. 27, pp. 1297–1328, 2006.

[12] S. Los *et al.*, "Vegetation height products between 60° S and 60° N from ICESat GLAS data," *Geosci. Model Develop.*, vol. 5, pp. 413–432, 2012.

[13] C. Mahoney, R. J. Hall, C. Hopkinson, M. Filiatrault, A. Beaudoin, and Q. Chen, "A forest attribute mapping framework: A pilot study in a northern boreal forest, Northwest Territories, Canada," *Remote Sens.*, vol. 10, 2018, Art. no. 1338.

[14] R. Dubayah *et al.*, "The global ecosystem dynamics investigation: High-resolution laser ranging of the earth's forests and topography," *Sci. Remote Sens.*, vol. 1, Jun. 2020, Art. no. 100002, doi: 10.1016/j.srs.2020.100002.

[15] P. Potapov *et al.*, "Mapping and monitoring global forest canopy height through integration of GEDI and Landsat data," *Remote Sens. Environ.*, vol. 253, 2021, Art. no. 100002.

[16] W. Wagner *et al.*, "Large-scale mapping of boreal forest in Siberia using ERS tandem coherence and JERS backscatter data," *Remote Sens. Environ.*, vol. 85, pp. 125–144, 2003.

[17] C. J. Thiel, C. Thiel, and C. C. Schmullius, "Operational large-area forest monitoring in Siberia using ALOS PALSAR summer intensities and winter coherence," *IEEE Trans. Geosci. Remote Sens.*, vol. 47, no. 12, pp. 3993–4000, Dec. 2009.

[18] G. Krieger *et al.*, "TanDEM-X: A satellite formation for high resolution SAR interferometry," *IEEE Trans. Geosci. Remote Sens.*, vol. 45, no. 11, pp. 3317–3341, Nov. 2007.

[19] M. Schlund, P. Magdon, B. Eaton, C. Aumann, and S. Erasmi, "Canopy height estimation with TanDEM-X in temperate and boreal forests," *Intl. J. Appl. Earth Observ. Geoinf.*, vol. 82, 2019, Art. no. 101904.

[20] P. da Conceicao Bispo *et al.*, "Mapping forest successional stages in the Brazilian Amazon using forest heights derived from TanDEM-X SAR interferometry," *Remote Sens. Environ.*, vol. 232, 2019, Art. no. 111194.

[21] S. Antonova *et al.*, "Estimating tree height from TanDEM-X data at the northwestern Canadian treeline," *Rem. Sens. Environ.*, vol. 231, 2019, Art. no. 111251.

[22] H. Chen, A. Beaudoin, D. A. Hill, S. R. Cloude, R. S. Skakun, and M. Marchand, "Mapping forest height from TanDEM-X interferometric coherence data in Northwest Territories, Canada," *Can. J. Remote Sens.*, vol. 45, no. 3/4, pp. 290–307, 2019.

[23] R. N. Treuhaft, S. N. Madsen, M. Moghaddam, and J. J. van Zyl, "Vegetation characteristics and underlying topography from interferometric radar," *Radio Sci.*, vol. 31, no. 6, pp. 1449–1485, 1996, doi: 10.1029/96RS01763.

[24] S. Cloude and K. Papathanassiou, "Polarimetric SAR interferometry," *IEEE Trans. Geosci. Remote Sens.*, vol. 36, no. 5, pp. 1551–1565, Sep. 1998.

[25] A. Olesk, K. Voormansik, A. Vain, M. Noorma, and J. Praks, "Seasonal differences in forest height estimation from interferometric TanDEM-X coherence data," *IEEE J. Sel. Top. Appl. Earth Observ. Remote Sens.*, vol. 8, no. 12, pp. 5565–5572, Dec. 2015.

[26] H. Chen, S. R. Cloude, and D. G. Goodenough, "Forest canopy height estimation using TanDEM-X coherence data," *IEEE J. Sel. Top. Appl. Earth Observ. Remote Sens.*, vol. 9, no. 7, pp. 3177–3188, Jul. 2016.

[27] H. Chen, S. R. Cloude, D. G. Goodenough, D. A. Hill, and A. Nesdoly, "Radar forest height estimation in mountainous terrain using Tandem-X coherence data," *IEEE J. Sel. Top. Appl. Earth Observ. Remote Sens.*, vol. 11, no. 10, pp. 3343–3352, Oct. 2018.

[28] Food and Agriculture Organization of the United Nations, *Global Forest Resources Assessment 2015: How Are the World's Forests Changing?* 2nd ed. Rome, Italy: Food Agriculture Org., 2015, p. 44.

[29] Food and Agriculture Organization of the United Nations, United Nations Environment Programme, Mediterranean Action Plan Barcelona Convention, Plan Bleu, *State of Mediterranean Forests 2018*. Marseille, France: Food Agriculture Org., 2018.

[30] D. Fernández Nogueira and E. C. Rico, "Cambios en los usos de suelo en la Península Ibérica: Un meta-análisis para el período 1985–2015," *Biblio3W Revista Bibliográfica de Geografía y Ciencias Sociales*, vol. 22, no. 1.215, pp. 1–29, 2017.

[31] C. Gómez, M. A. Wulder, J. C. White, F. Montes, and J. A. Delgado, "Characterizing 25 years of change in the area, distribution, and carbon stock of Mediterranean pines in Central Spain," *Int. J. Remote Sens.*, vol. 33, no. 17, pp. 5546–5573, 2012.

[32] G. Moreno, J. J. Obrador, E. Cubera, and C. Dupraz, "Fine root distribution in Dehesas of Central-Western Spain," *Plant Soil*, vol. 277, pp. 153–162, 2005, doi: 10.1007/s11104-005-6805-0.

[33] I. Alberdi *et al.*, "The multi-objective Spanish national forest inventory," *Forest Syst.*, vol. 26, no. 2, 2017, Art. no. e04S, doi: 10.5424/fs/2017262-10577.

[34] MAPAMA, Forest Statistical Annual Report, Ministry of Agriculture, Food and Environment, Madrid, Spain, p. 103, 2011.

[35] R. Vallejo-Bombín, "The Spanish Forest Map scale 1:50000 (MFE50) as base for the third national forest inventory," (in Spanish) *Cuad. Soc. Esp. Cienc. For.*, vol. 19, pp. 205–210, 2005.

[36] A. Arozarena *et al.*, "The Spanish National Territory Observation Program: current states and next steps," (in Spanish) *Mapping Inter.*, vol. 111, pp. 16–22, 2006.
[37] A. Olesk, J. Praks, O. Antropov, K. Zalite, T. Arumae, and K. Voormansik, "Interferometric SAR coherence models for characterization of hemiboreal forests using TanDEM-X data," *Remote Sens.*, vol. 8, no. 9, 2016, Art. no. 700.
[38] J. M. Lopez-Sanchez, F. Vicente-Guijalba, E. Erten, M. Campos-Taberner, and F. J. García-Haro, "Retrieval of vegetation height in rice fields using polarimetric SAR interferometry with TanDEM-X data," *Remote Sens. Environ.*, vol. 192, pp. 30–44, 2017.
[39] F. Kugler, D. Schulze, I. Hajnsek, H. Pretzsch, and K. P. Papathanassiou, "TanDEM-X Pol-InSAR performance for forest height estimation," *IEEE Trans. Geosci. Remote Sens.*, vol. 52, no. 10, pp. 6404–6422, Oct. 2014.
[40] K. P. Papathanassiou and S. R. Cloude, "Single-baseline polarimetric SAR interferometry," *IEEE Trans. Geosci. Remote Sens.*, vol. 39, no. 11, pp. 2352–2363, Nov. 2001.
[41] R. N. Treuhaft and P. R. Siqueira, "The vertical structure of vegetated land surfaces from interferometric and polarimetric radar," *Radio Sci.*, vol. 35, pp. 141–177, Jan. 2000.
[42] H. Persson, H. Olsson, M. Soja, L. Ulander, and J. Fransson, "Experiences from large-scale forest mapping of Sweden using TanDEM-X data," *Remote Sens.*, vol. 9, no. 12, Dec. 2017, Art. no. 1253.
[43] X. Wang and H. Wang, "Forest height mapping using complex-valued convolutional neural network," *IEEE Access*, vol. 7, pp. 126334–126343, 2019.
[44] W. Qi and R. O. Dubayah, "Combining Tandem-X InSAR and simulated GEDI lidar observations for forest structure mapping," *Remote Sens. Environ.*, vol. 187, pp. 253–266, 2016.
[45] W. Qi *et al.*, "Improved forest height estimation by fusion of simulated GEDI lidar data and TanDEM-X InSAR data," *Remote Sens. Environ.*, vol. 221, pp. 621–634, 2019, doi: 10.1016/j.rse.2018.11.035.

Cristina Gómez received the M.Sc. degree in applied geospatial technologies from the University of Aberdeen, Aberdeen, U.K., in 2006, and the Ph.D. degree in conservation and sustainable use of forest systems from the University of Valladolid, Valladolid, Spain, in 2014.

She is an M.Sc. Forest Engineer at the Technical University of Madrid, Madrid, Spain, in 2001. Her current research focuses on the characterization and monitoring of environmental dynamics at different spatio–temporal scales, integrating a range of geospatial technologies. She employs time-series analysis of remotely sensed data for assessment of forest processes of change, like drastic and subtle disturbance, or natural succession including regeneration, growth, decline, and mortality. She is particularly interested in forest phenological traits and variations through time, as well as long-term trends of change to help assessing forest structure and ecosystemic services.

Juan M. Lopez-Sanchez (Senior Member, IEEE) received the Ingeniero (M.S.) and Doctor Ingeniero (Ph.D.) degrees in telecommunication engineering from the Technical University of Valencia, Valencia, Spain, in 1996 and 2000, respectively.

From 1998 to 1999, he was a Predoctoral Grantholder with the Space Applications Institute, Joint Research Centre of the European Commission, Ispra, Italy. Since 2000, he has been leading the Signals, Systems and Telecommunication Group, University of Alicante, Alicante, Spain, where he has been a Full Professor since November 2011. His research interests include microwave remote sensing for inversion of biophysical parameters, polarimetric and interferometric techniques, SAR imaging algorithms, and applications of radar remote sensing in agriculture and geophysics.

Dr. Lopez-Sanchez was the recipient of the Indra Award for the Best Ph.D. Thesis about radar in Spain in 2001. From 2006 to 2012, he was the Chair of the Spanish Chapter of the IEEE Geoscience and Remote Sensing Society. He has coauthored more than 80 papers in refereed journals and more than 130 papers and presentations in international conferences and symposia.

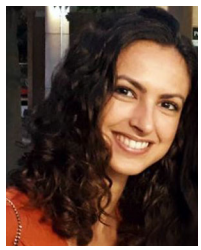

Noelia Romero-Puig (Student Member, IEEE) received the B.Sc. degree in sound and image in telecommunications engineering, in 2016 and M.Sc. degree in telecommunication engineering, in 2018 from the University of Alicante, Alicante, Spain, where she is currently working toward the Ph.D. degree in the field of signal processing and telecommunications at the Signal, Systems and Telecommunications Group.

Her current research focuses on the monitoring of agricultural crops by means of InSAR and PolInSAR techniques.

Miss Romero-Puig was the recipient of the Award for Best Final Master's Project in Remote Sensing defended in Spain during 2018 of the IEEE GRSS Spanish Chapter, and the Hisdesat Award for the Best Final Master's Project in Government Satellite Services by the Official College of Telecommunications Engineers.

Jianjun Zhu received the M.Eng. degree in engineering surveying and Ph.D. degree in geodesy and surveying engineering from the Central South University of Technology (now Central South University), Changsha, China, in 1985 and 1998, respectively.

From 1998 to 1999, he was a Research Assistant with the Department of Land Surveying and GeoInformatics, The Hong Kong Polytechnic University, Hong Kong. From 2000 to 2001, he was a Postdoctoral Fellow with the Center for Research on Geomatics, Laval University, Québec City, QC, Canada. He is currently a Full Professor with the School of Geosciences and Info-Physics, Central South University. His research interests include the theory of errors and surveying adjustment and its applications in interferometric satellite synthetic aperture radar.

Haiqiang Fu received the bachelor's degree in remote sensing science and technology from Southwest Jiaotong University, Chengdu, China, in 2011, and the master's and Ph.D. degrees in geodesy and survey engineering from Central South University, Changsha, China, in 2014 and 2018, respectively.

He is currently an Associate Professor with the School of Geosciences and Info-Physics, Central South University. His research interests include Pol-SAR interferometry and its applications for monitoring forest parameters and extracting the underlying topography over forest areas.

Wenjie He received the bachelor's and the master's degrees in geodesy and survey engineering, in 2011 and 2015, respectively, from Central South University, Changsha, China, he is currently working toward the Ph.D. degree in geodesy and surveying engineering.

His research interests include PolSAR interferometry and its applications for monitoring forest parameters over forest areas.

Yanzhou Xie received the bachelor's degree in geodesy and survey engineering, in 2018, from Central South University, Changsha, China, where he is currently working toward the Ph.D. degree in geodesy and surveying engineering.

His research interests include data processing and algorithms for polarimetric SAR interferometry and its applications for extracting forest parameters and retrieval of the underlying topography over forest areas.

Qinghua Xie received the bachelor's degree in surveying engineering and Doctor degree in geodesy and surveying engineering from Central South University, Changsha, China, in 2010 and 2017, respectively.

From 2014 to 2016, he was a Visiting Ph.D. Student with the University of Alicante, Alicante, Spain. From 2018 to 2019, he was a Postdoctoral Associate with The University of Western Ontario, London, ON, Canada. He is currently an Associate Professor with the School of Geography and Information Engineering, China University of Geosciences, Wuhan, China. His research interests include modeling and interpretation of scattering mechanisms polarimetric synthetic aperture radar, polarimetric and interferometric techniques for inversion of biophysical parameters over forest, and agricultural areas.